Freely Suspended Cellular "Backpacks" Lead to Cell Aggregate Self-Assembly

Albert J. Swiston,[†] Jonathan B. Gilbert,[‡] Darrell J. Irvine,[†,§,ǁ] Robert E. Cohen,[‡] and Michael F. Rubner*,[†]

Departments of Materials Science and Engineering, Biological Engineering, and Chemical Engineering, Massachusetts Institute of Technology, Cambridge, Massachusetts 02139, and Howard Hughes Medical Institute, Chevy Chase, Maryland 20815

Cellular "backpacks" are a new type of anisotropic, nanoscale thickness microparticle that may be attached to the surface of living cells creating a "bio-hybrid" material. Previous work has shown that these backpacks do not impair cell viability or native functions such as migration in a B and T cell line, respectively. In the current work, we show that backpacks, when added to a cell suspension, assemble cells into aggregates of reproducible size. We investigate the efficiency of backpack–cell binding using flow cytometry and laser diffraction, examine the influence of backpack diameter on aggregate size, and show that even when cell–backpack complexes are forced through small pores, backpacks are not removed from the surfaces of cells.

Introduction

There exists a new, burgeoning field of biohybrid materials in which synthetic materials are functionally integrated with cellular species while leveraging both biological and material properties and behaviors. Synthetic materials systems such as anisotropic microparticles,[1] muscular thin films,[2] thermally responsive films with integrin ligands,[3] films capable of sensing and selectively releasing dead cells,[4] magnetic micromanipulators,[5] nanoparticulate cellular patches,[6] and functional cell backpacks[7] have recently been reported offering exciting possibilities for a new class of biomaterials based on the symbiosis between synthetic building blocks and native biological behavior.

Cellular "backpacks" are nanoscale thickness, micrometer-sized, photolithographically patterned heterostructured multilayer systems capable of noncytotoxically attaching to the membrane of a living cell.[7] Cellular backpacks have been attached to the surface of two types of living immune cells without impairing their native behaviors. If a backpack is attached to a cell that normally performs a useful function, such as homing to solid tumors or areas of trauma, then these native behaviors can be leveraged to deliver functional materials contained within the backpack. Diagnostic (such as imaging) or therapeutic (such as delivery) payloads are possible, as well as combining several modalities in a single platform.

Each backpack contains a functional payload which may be any material that can be integrated in multilayer or homopolymer thin films, including drugs, imaging contrast agents, and nanoparticles. The attachment mechanism between the backpack and the cell surface must be chosen based on the cell type of interest. In this work, we used a B cell line that expresses an abundance of the cell surface receptor CD44, for which the natural ligand is hyaluronic acid (HA). One face of the backpack consists of a HA-containing multilayer that attaches to the membrane of one or more cells.

In previous work,[7] backpacks were fabricated on a glass slide and tethered to the substrate via a pH- and temperature-labile region. Cells were attached to backpacks at a controlled ratio (R = No. of cells/No. of backpacks) via the CD44-HA interaction and released upon lowering the temperature. This yielded cell–backpack complexes with a well-defined number of cells and backpacks. While this technique afforded great control over cell–backpack association, the effort-intensive process of seeding and releasing on a 2D surface may limit its clinical relevancy. An alternative method is one where the backpacks are released and collected from the fabrication substrate ex vivo and exposed to cell suspensions. We refer to this approach as an injectable formulation because backpack solutions could easily be loaded into a syringe and injected into a patient. Because injectable backpacks are free to attach to cells in many different configurations, including multiple cells per backpack and vice versa, cell–backpack aggregates form.

Suematsu et al.[8] recently reported forming immune cell aggregates for tissue engineering applications. A collagen scaffold seeded with stromal cells was transplanted into mice. This traditional tissue engineering approach produced artificial lymphoid-like organoids that functioned much like secondary lymphoid organs, recruiting B and T cells and forming follicular dendritic cell networks. This work offers exciting possibilities in engineering hybrid synthetic-biological devices for treating immunodeficiency diseases. Their approach, however, requires surgical implantation techniques for introducing the lymphoid-like tissue into the body, and much greater clinical ease may be found in methods able to form organoids by simply injecting a cell-containing suspension.

Cellular backpacks may offer an alternative strategy to create injectable synthetic lymphoid organoids that achieve the extremely high cell density typical of lymphoid tissues. Cells could be mixed with backpacks to form aggregates that may be passed through small pores (for example, a needle tip), disaggregate, and dynamically reform. Because the backpacks do not occlude the entire cell surface, cells are free to interact with the environment, an essential requirement for immune system components. Motivated by the work of Suematsu et al. and our

---

* To whom correspondence should be addressed. E-mail: rubner@mit.edu.
† Department of Materials Science and Engineering.
‡ Department of Chemical Engineering.
§ Department of Biological Engineering.
ǁ Howard Hughes Medical Institute.

original observation that cells would aggregate upon freely suspended backpack exposure, we sought to create cellular aggregates that are reversibly associated but with enough cell−backpack association strength to withstand mechanical challenges.

In this paper, we present fundamental studies on forming cellular aggregates using injectable cellular backpacks, how to control aggregate size, and observations on cell−backpack association strength. We found that two parameters strongly determined the size and character of aggregates: the ratio of cells to backpacks in a culture and the diameter of the backpack. Using confocal microscopy, flow cytometry, and laser diffraction, we observed that, while very large (>1 mm) aggregates can form, aggregates may also dissociate and reform. Aggregates were forced through a nylon mesh filter and observed afterward: as the filter size decreased, resulting aggregates were smaller. For a pore size less than the diameter of the cell, backpacks were still attached, perhaps indicating a sufficiently strong cell−backpack association required for a backpack to remain attached to a lymphocyte undergoing extravasation in vivo. We feel that an injectable backpack system could have applications in lymphoid tissue engineering as described by Suematsu,[8] as well as more general cellular engineering applications requiring close cell association.

Materials and Methods

Materials. Poly(methacrylic acid) (PMAA, PolySciences, $M = 100$ kDa), poly(vinylpyrrolidone) (PVPON, Aldrich, $M = 1.3$ MDa), poly(diallyldimethylammonium chloride) (PDAC, Aldrich, $M = 200-350$ kDa in 20% aqueous solution), poly(styrene sulfonate) (SPS, Aldrich, $M = 70$ kDa), hyaluronic acid (HA, Fluka, from *Streptococcus equi*, Fluka, $M \sim 145$ kDa by intrinsic viscosity[9]), low MW chitosan (CHI, Sigma, DS = 0.85, $M \sim 390$ kDa by intrinsic viscosity[10]), and poly(lactide-*co*-glycolide) (PLGA, Sigma, $M_w = 5-15$ kDa) were used without purification. Cells were passaged and maintained in RMPI with L-glutamine (Mediatech), penicillin/streptomycin (P/S, Mediatech), and fetal calf serum (characterized FCS, Mediatech). 3,3′-Dioctadecyloxacarbocyanine perchlorate (DiO, Molecular Probes), which fluoresces at the same wavelengths as fluorescein isothiocyanate (FITC), was used to stain the PLGA backpack. Iron oxide magnetic nanoparticles (MNP, Fe_3O_4, 10 nm diameter, Ferrotec EMG 705) stabilized with an anionic surfactant were used. Hank's Balanced Salt Solution (Gibco) was used to wash cells, and propidium iodine (PI, Calbiochem) was used as a viability dye. Additional information on solution concentrations and pH conditions used during depositions can be found in the Supporting Information.

Backpack Fabrication. We used a previously described[7] aqueous-based layer-by-layer technique to deposit the polymer films. One significant exception is the PLGA region of the backpack in the current study, which was assembled using a spray technique. A solution of PLGA (1 mg/mL) and DiO (1 mg/mL) in chloroform was sprayed (10 mL/min for 30s, substrate 15 cm from a Badger 105 air brush powered with nitrogen) onto the surface of a $(PMAA2.0/PVPON2.0)_{20.5}$ multilayer atop a patterned photoresist layer. The resulting thickness was ∼10 nm, as observed by spraying PLGA onto Si wafers and measuring using spectroscopic ellipsometry.[11] Chloroform does not dissolve the developed photoresist. Substrates were then coated by the layer-by-layer technique to build the rest of the heterostructured, functional backpack. The following formula describes all backpacks used in this work: $(PMAA2.0/PVPON2.0)_{20.5}(PLGA+DiO)(PAH3.0/MNP4.0)_{10}(CHI3.0/HA3.0)_3$, where the number following each LbL deposited species indicates the solution pH and subscripts are the number of bilayers (where a half bilayer is indicated as 0.5). We included a $(PAH3.0/MNP4.0)_{10}$ layer to increase the mechanical integrity of the backpack; we found that backpacks built identically but without the $(PAH3.0/$

$MNP4.0)_{10}$ region were compromised during acetone sonication, as indicated by a lack of DiO signal. The $(CHI3.0/HA3.0)_3$ region was built with 100 mM NaCl added to each polymer solution. To detach backpacks from the glass substrate, 1 mL of PBS was pipetted onto the surface and a cell scraper was used to gently remove the backpacks. The backpacks in PBS were collected with a pipet and passed through a 27 μm nylon mesh (McMaster Carr) to remove any large aggregates or backpacks that had not correctly undergone acetone liftoff.

Cell Culture. CH27 B-lymphocytes were maintained at 37 °C, 5% CO_2, and passaged in RPMI 1640 cell culture media (Mediatech) supplemented with 10% FCS, 1% penicillin/streptomycin, and 25 mM HEPES.

Backpack Attachment. Cells were washed once with HBSS and resuspended at 10^6 cells/mL in complete RPMI media. Backpacks were pelleted down (2000 rpm for 5 min) and resuspended in PBS at 10^7 backpacks/mL (as measured by a hemacytometer). We did not observe backpack flocculation during this centrifugation and resuspension processing. For imaging and laser diffraction experiments, backpacks were introduced at the indicated ratio to the cell suspension in 4 or 8 well LabTek chambers (Nunc) and agitated at ∼100 rpm at 37 °C and 5% CO_2 for 15 min, incubated for 15 min in the same conditions, and this cycle was repeated once more. Cells were allowed to sediment down for ∼30 min before imaging. For flow cytometry experiments, the concentration of cells in complete media was 10^6 cells/mL, and the backpack concentration in PBS was 6×10^6 backpacks/mL. Backpacks were introduced to the cells in 35 mm Petri dishes, which were agitated as described above. Cell−backpack aliquots were transferred to 15 mm tubes and chilled on ice.

Flow Cytometry and Confocal Microscopy. Aliquots of cell−backpack complexes were analyzed on a BD FACS Canto II flow cytometer. The cell viability marker propidium iodide (PI, 50 μg/mL PBS) was added during backpack attachment at 40 μL/10^6 cells (i.e., a final 2 μg/mL PI concentration with 10^6 cells/mL). Data sets of 1×10^5 events were gated so that only sufficiently large objects were analyzed (i.e., above the FSC value for a B cell) and further gated on a low PI signal (i.e., only live cells). Confocal laser scanning microscopy images were collected on an inverted Zeiss LSM 510 using 4 or 8 well LabTek chambers and a 10× air objective under ambient conditions. Because the exact shape and structure of each aggregate is of less interest than the overall size and frequency, most microscopy data is shown at low magnification so that multiple aggregates may be seen in each field of view. These images are an overlay of brightfield and fluorescence signals, and the reader is directed to note the green aggregates. Though green fluorescence arises from the DiO cosprayed with PLGA, FITC detectors were used on the flow cytometer and confocal microscope and data is thus labeled "FITC" throughout this work.

Particle Size Measurement by Laser Diffraction. Cell−backpack complexes were analyzed using a Horiba LA-950 V2 laser diffraction system. Cell−backpack aliquots at the indicated ratio were gently added to 18 mL pH 7.4 PBS in a quartz cuvette. Data were collected before and after gentle agitation using the built-in magnetic stir bar. All data shown were collected following agitation. Data analysis was performed using a Fraunhofer model,[12] which does not require the input of a refractive index.

Nylon Mesh Filtering. Backpacks were attached to cells at $R = 0.33$, and 0.5 mL aliquots were passed through 25 mm diameter nylon mesh filters of three different opening sizes (20, 30, and 60 μm; Millipore) using a reusable syringe filter (Pall). These aliquots were placed in 4 well LabTek chambers and observed using confocal microscopy.

Results and Discussion

Backpacks were assembled on a glass substrate using a photolithographic lift-off technique.[13,14] Photoresist was deposited and patterned with 7 or 15 μm circles on a $(PDAC4/SPS4)_{15.5}$-coated glass slide, which was then coated using a
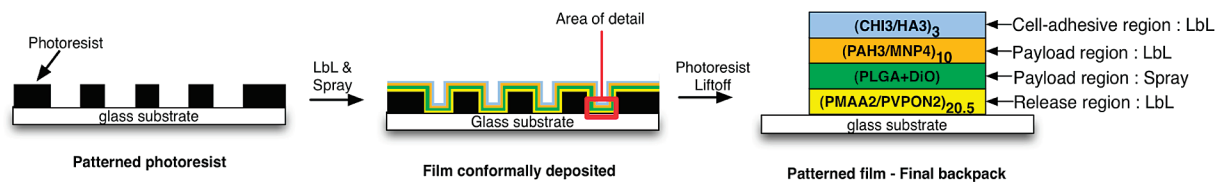
Figure 1. Schematic overview of backpack fabrication, including the composition and deposition method for each lamellar region.

combination of two different methods. A number of sequential, layer-by-layer (LbL) deposition techniques are possible, including spin assembly,[15] spraying,[16−18] and dip-coating deposition.[19−21] We used traditional dipping LbL deposition for most regions of the backpack system and an airbrush spraying method to create the backpack's biodegradable PLGA payload region. PLGA is known as an ideal delivery system as it degrades at physiological conditions into bioresorbable products.[22] We added DiO, a hydrophobic fluorescent dye, to the payload region for visualization. Chloroform was chosen as the mutual PLGA/DiO solvent since it did not dissolve the release region (described below) or the patterned photoresist. We are able to build a functional backpack that contains a PLGA payload, along with any functional component that may be integrated into a PLGA homopolymer film. Traditional LbL dipping was used to build the rest of the backpack. An overview of the backpack fabrication process, including which assembly technique was used for each region, is shown in Figure 1. The thicknesses of each region is approximately 250 nm for the release region, 10 nm for the (PLGA+DiO) payload, 100 nm for the (PAH3.0/MNP4.0)$_{10}$ region, and 30 nm for the (HA3.0/CHI3.0)$_3$ cell-adhesive strata.

The backpack's release region attaches the functional payload to the glass substrate and is labile under certain conditions. Previously,[7] this region was based on a hydrogen-bonded poly(*N*-isopropylacrylamide) (PNIPAAm) system found to be labile only below PNIPAAm's lower critical solution temperature (LCST, ~32 °C[23]) and above a critical pH (~6.2[20]). Cells were seeded onto the surface-bound backpacks at a ratio of 1:1 (depending on the backpack diameter), which minimized cell−backpack aggregation upon release. While imposing a one-backpack-per-cell association condition is useful, there is much greater clinical ease in a system where the backpack is released prior to cell exposure. In this work, we used a backpack release region based on poly(methacrylic acid) (PMAA) and poly(vinylpyrrolidone) (PVPON), which dissolves and releases the backpack above pH ~ 6.4.[20] As shown previously,[20] this critical dissolution pH is due to the deprotonation of PMAA carboxylic acids, which are participating in hydrogen bonds. When this mechanism is used, backpacks can be released from the fabrication substrate and collected, then attached to cells in an ex vivo cell culture or injected directly into the body where cells of interest may bind to specific ligands on the backpack surface.

An "injectable" backpack formulation, however, leads to cell−backpack aggregates. These aggregates contain any number of cells and backpacks, and the factors influencing the order of these aggregates include the number of cells per backpack and the number of backpacks attached to each cell. Nonconformal attachment can occur due to curvature of the flexible backpack; an overhanging portion of the backpack may then bind to one or more cells. An example is shown in Figure 2a, where three cells attached to a single backpack. When a single cell is associated with more than one backpack, and each backpack may attach multiple cells, aggregates form. Figure 2b shows one of the lowest order aggregates that may form, where one
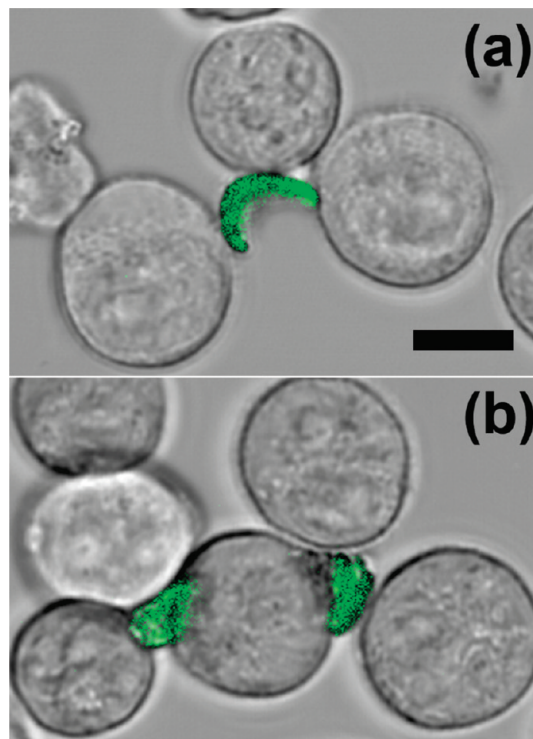

Figure 2. Confocal microscopy images of ways B cells attached to backpacks using the injectable backpack protocol. (a) How a 7 μm backpack may attach to several cells and (b) how each cell may bind to more than one backpack. Scale bar is 10 μm, and $R = 10$ for both aliquots. The green fluorescence signal is from the DiO sprayed with PLGA.

cell has two backpacks and each backpack has three cells attached. Each of these micrographs shows cells exposed to backpacks for ~1.5 h, and no evidence of internalization was ever observed. (In fact, when backpacks are exposed to a macrophage cell line known to quickly internalize spherical particles several micrometers in diameter, we see very little backpack internalization. This is the subject of ongoing investigation and will be featured in an up-coming publication.)

As will be shown later, aggregate size depends on (1) the number of cells associated per backpack and (2) the number of backpacks per cell. Backpack size, controllable during fabrication, will strongly influence the number of cells associated per backpack[7] (see Figure 2a,b). We fabricated backpacks of two different diameters ($d = 7$ and 15 μm) and controlled the number of backpacks associated per cell by changing the ratio of cells to backpacks (R = No. of cells/No. of backpacks). We find that aggregate size monotonically decreases with R and increases with d (for a given R).

Figure 3 shows flow cytometry plots and confocal micrographs of cell−backpack ($d = 7$ μm) aliquots for $R = 1−0.1$ (for easier visualization, similar plots and micrographs for $R = 10−3$ may be found in the Supporting Information). Shown are FITC signal versus forward scatter (FSC) data from flow cytometry: cell aggregates are detected at higher FSC, and
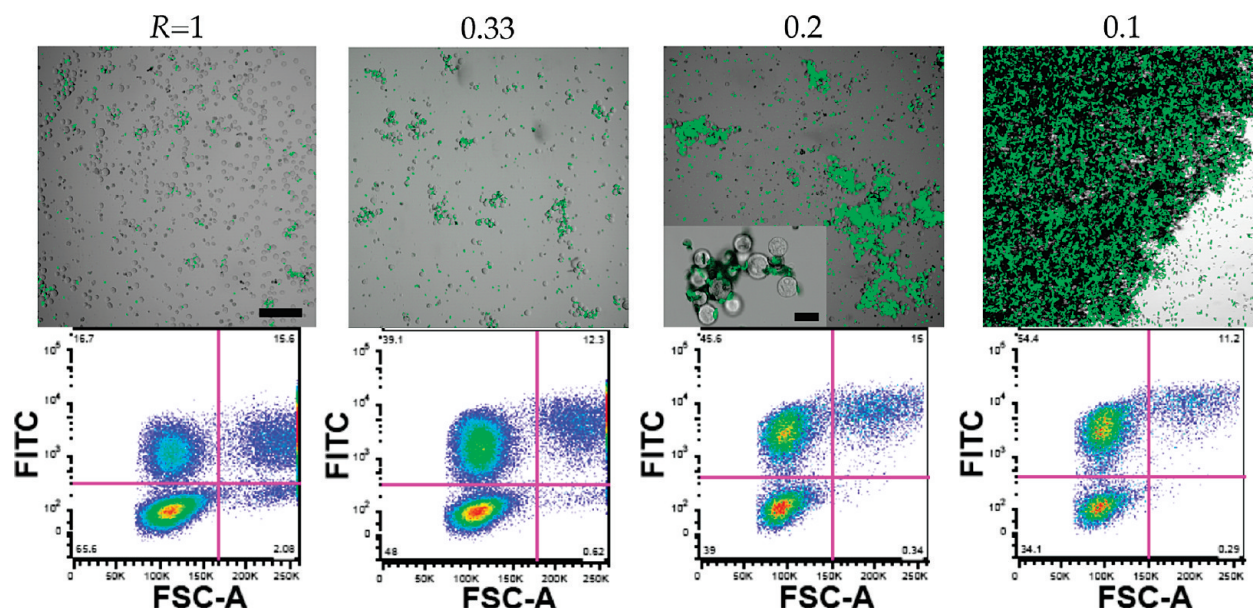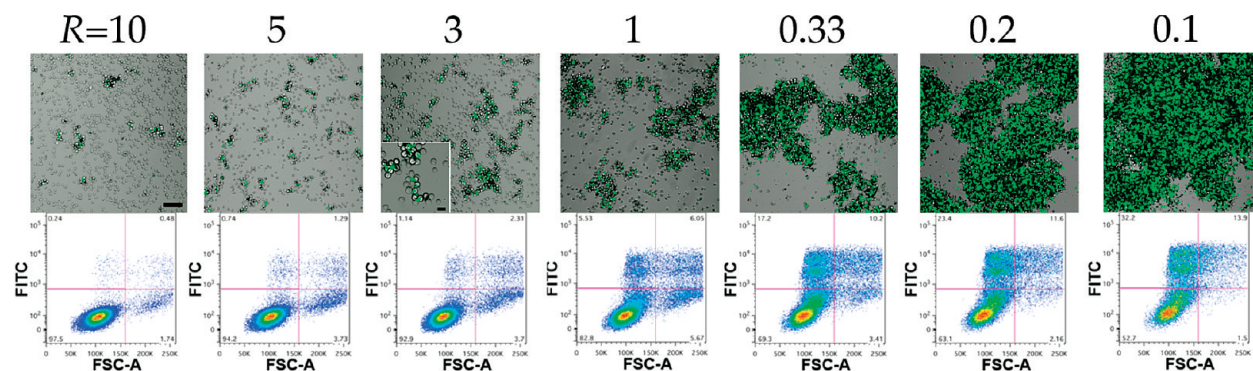
Figure 3. Confocal microscopy images and flow cytometry plots (FITC vs FSC) of aggregates formed under different cell to backpack ratios (R = 1−0.1). The diameter of each backpack is 7 μm. A higher magnification view of a cell−backpack aggregate is provided for R = 0.2. Scale bar is 100 μm (inset scale bar for R = 0.2 is 20 μm).

Figure 4. Confocal microscopy images and flow cytometry plots (FITC vs FSC) of aggregates formed under different cell-to-backpack ratios (R = 10−0.1). The diameter of each backpack is 15 μm. A higher magnification view of a cell−backpack aggregate is provided for R = 3. Scale bar is 100 μm (inset scale bar for R = 3 is 20 μm).

aggregates associated with one or more backpacks are detected at higher FITC values (since each backpack contains DiO in the PLGA region, which fluoresces almost identically to FITC). Thus, aggregates with backpacks are found in the upper right quadrant, and single cells with one or more backpacks are found in the upper left quadrant. We used confocal microscopy to directly observe aggregate size, which dramatically increases with decreasing R. For $R > 1$, we see very small aggregates (less than three cells), with primarily only one backpack associated per cell (see Supporting Information for confocal micrographs and flow cytometry plots). At $R = 1$, larger aggregates begin to form, and by $R = 0.2$, large complexes are found. At $R = 0.1$, a single aggregate formed in the dish; the micrograph in Figure 3 shows only the edge of this aggregate. To further quantify these aggregate structures, flow cytometry analysis of backpack fluorescence versus FSC on cell−backpack aliquots shows that as R decreases, the number of cells associated with a backpack increases. Because the flow cytometer passes the cell suspension through a small quartz capillary, aggregates break up before passing through the laser path for analysis. This limits analysis to small aggregates, single cells, and single backpacks (which are excluded from this analysis based on PI signal and FSC value), though the starting aliquot

included large aggregates. As laser diffraction data indicates, the large aggregates seen in the optical images below are associated via both strong, specific, CD44-HA interactions and weak, nonspecific, cell−backpack binding. Small clusters, as seen in Figure 2, associate only via the strong CD44-HA interactions, and these are the FSC^{high} events shown in Figures 3 and 4. A detailed discussion of how different association strengths lead to large aggregates versus small cell clusters is presented along with the laser diffraction data below.

The backpack diameter d also strongly influences the size of aggregates. Figure 4 shows confocal images and flow cytometry plots of cell−backpack aggregates formed with $d = 15$ μm backpacks. Aggregate size trends are similar to the $d = 7$ μm case, but the onset R value at which aggregation begins increases to greater than $R = 10$. Indeed, the aggregates seen for $d = 7$ μm and $R = 0.33$ are roughly the same size as those seen for $d = 15$ μm and $R = 10$. This suggests a superposition of the d (backpack diameter) and R (number of backpacks per cell) variables.

As can be seen in Figure 3, FITC^{high} events have two distinct populations differing by a factor of 2 in FSC intensity. This reflects single cells with a backpack or small aggregates with one or more backpacks associated. Figure 5 shows the percent-
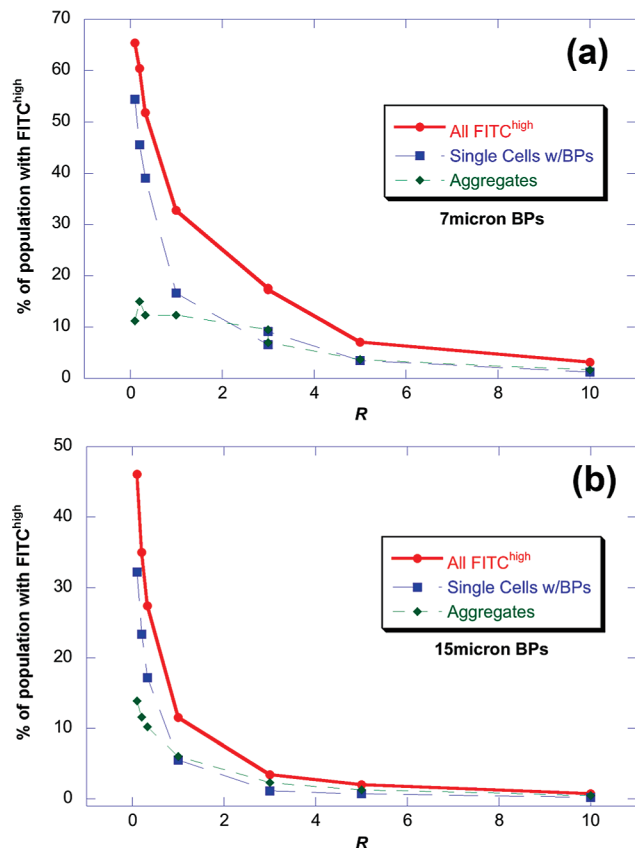
Figure 5. Plots summarizing the flow cytometry results in Figures 3 and 4. The total percentage of FITC[high] events, which represents an attached backpack, are plotted vs R for (a) $d = 7$ μm and (b) $d = 15$ μm backpacks. As R increases, the number of cells associated with a backpack monotonically decreases. The values here probably represent a lower bound of the actual value of cells with backpacks (see text for discussion).

Figure 6. Examples of how some $d = 15$ μm backpacks curl upon themselves: (a) a cylindrical folding; (b) a "tricorne"-like shape. Scale bar is 10 μm.

Figure 7. Aggregate size distributions for (a) $d = 7$ μm and (b) $d = 15$ μm backpacks. These curves show two populations, one centered at ~15 μm (single CH27 cells) and the other at an increasingly greater diameter, depending on R. For $d = 7$ μm backpacks, a clear second peak appears at $R = 1$; this second peak appears at $R = 3$ for $d = 15$ μm backpacks. Individual, nonbackpacked CH27 cells are shown as the dashed line.

age of FITC[high]FSC[low] (single cells with a backpack) and FITC[high]FSC[high] (small clusters) events, as well as the sum, for both $d = 7$ and 15 μm. For $d = 7$ μm, at $R = 10$, 3% of cells are associated with a backpack; at $R = 0.1$, 65% of events include a backpack. When the diameter increases to 15 μm, the highest number of cells with an attached backpack decreases to 46%. While this might reflect slight differences in sample handling, it is more likely that this decrease is due to curling of some backpacks upon themselves, thus, reducing the total surface area available to strongly bind. Examples of how $d = 15$ μm backpacks fold are seen in Figure 6. This curling behavior was not observed for $d = 7$ μm backpacks, suggesting some critical size required for folding.

As cells pass through the cytometer's fluidics system, the solution is forced through a small capillary. The values reported in Figure 5 are lower bound estimates for the true number of cells associated with backpacks, because some backpacks will be sheared off the surface of cells during flow through the instrument.

We used laser diffraction to further quantify the nature of these aggregates and investigate their association strength. Aliquots of cell−backpack complexes mixed at the same ratios as above show increasingly large aggregates with decreasing R, which agrees with the confocal microscopy results presented above. Unlike the confocal results, all diffraction samples were mildly agitated (at about 100 rpm using a built-in stir bar) before analysis. Prior to agitation, most samples show an extremely large aggregate distribution curve (mean > 1 mm) that is not

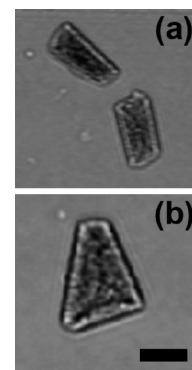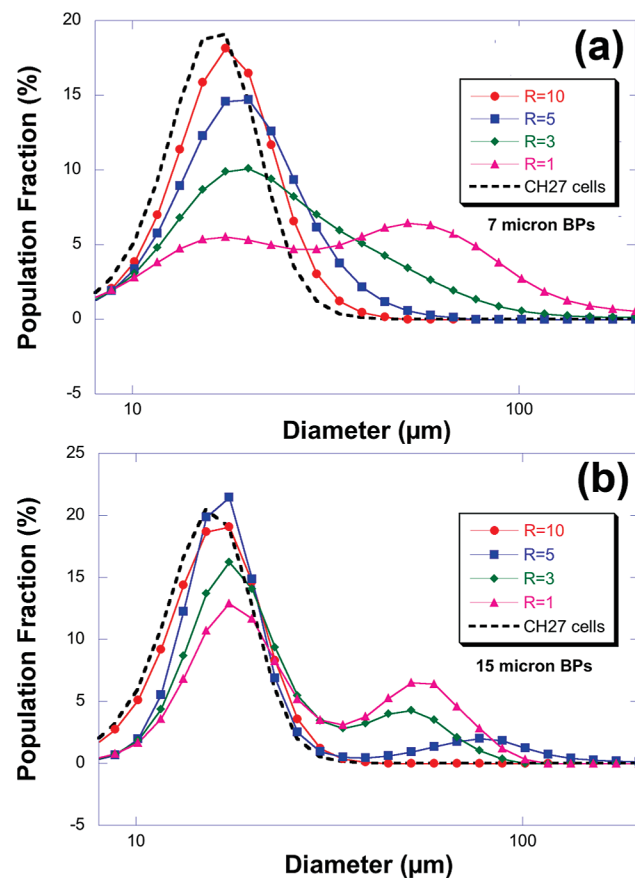constant with time; very large fluctuations led to inconsistent data. Upon agitation, this distribution falls to the curves shown in Figure 7, which are consistent and reproducible. Furthermore, if agitation was stopped, the large aggregate distribution appeared again, showing that aggregate dissociation is reversible. An agitation-dependent distribution for $R = 0.33$ is provided in the Supporting Information, as well as confocal microscopy images of before- and after-agitation aliquots.

In Figure 7, B cells are shown as the dashed line, which has a distribution mean of ~15 μm, slightly smaller than the 17
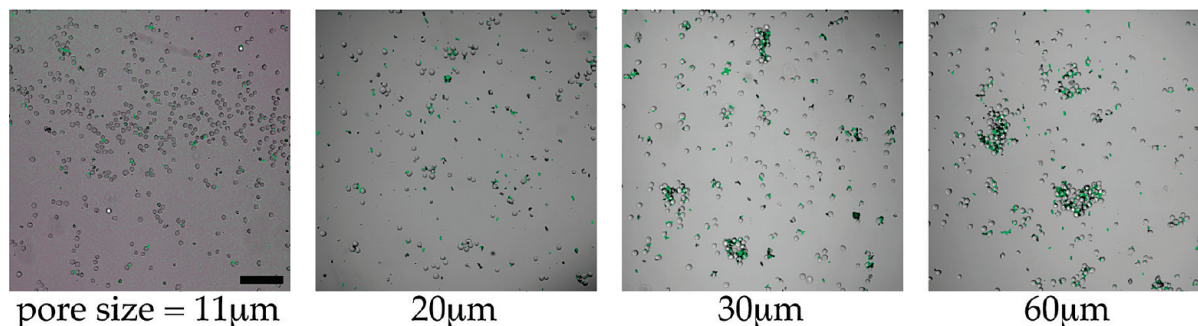
Figure 8. Confocal microscopy images of aggregates seen after filtering a $R = 0.33$, $d = 7$ μm aliquot through the indicated mesh pore sizes. As the mesh size decreases, so does the resulting aggregate size. Scale bar is 100 μm.

μm cell diameter observed by microscopy. At $R = 10$, we see a similarly shaped curve shifted to the right, suggesting one-backpack-to-cell complexes. As R decreases, multicell, multi-backpack aggregates begin to form, both shifting the mean value higher and changing the shape of the curve to include a broad shoulder. At $R = 1$ for $d = 7$ μm and $R = 3$ for $d = 15$ μm, a second peak emerges, indicating a distinct aggregate population. Consistent with the confocal results above, as d increases the aggregation-onset R value increases as well.

From the flow cytometry and laser diffraction data, we find that aggregates are able to dissociate into smaller cell-backpack clusters. The number of cells in each cluster depends on R and d, and these clusters weakly bind together to form the large aggregates seen in Figures 3 and 4. Additionally, this association−dissociation event is reversible; once agitation is stopped, very large aggregates were observed again. The association in a small cell cluster is based on CD44-HA interactions between the membrane and the HA-containing cell-adhesive region. Binding between clusters to form large aggregates are much weaker and is likely based on nonselective interactions between cells and the outer face of the backpack (which contains some or all of the hydrogen-bonded release region). These nonselective interactions are weak enough to be compromised with even mild agitation. Binding interactions in the small cell clusters, however, are not compromised by even very harsh agitation (maximum stir bar rotation).

To further test how strongly backpacks are attached to B cells in clusters and aggregates, aliquots of cells and backpacks ($R = 0.33$, $d = 7$ μm) were collected and passed through nylon mesh filters of varying aperture size. This experiment provides a rough approximation of extravasation, the process by which immune system cells leave the circulatory system and enter tissue. This process requires the cells to squeeze through very tightly apposed endothelial cells,[24] exerting shear forces on the surface and challenging the adherence of any attached object.

The average diameter of a B cell is ∼17 μm, and four mesh sizes were chosen to challenge the aggregate association strength as well as the cell−backpack interaction. Figure 8 shows that, for mesh opening sizes of 11, 20, 30, and 60 μm, a significant number of cell−backpack complexes remain after filtering. Consistent with the agitation-dependent, reversible aggregation behavior seen above, aggregates are dissociating into smaller aggregates or cell clusters (i.e., cells attached to a backpack via strong CD44-HA interactions) while passing through the mesh. (The total number of cells in the filtrate is comparable to the prefiltered aliquot, indicating that very few clusters or aggregates are actually removed during filtering.) After this dissociation, small aggregates and clusters are then free to reform larger aggregates. The size of the remade aggregates decreases with decreasing mesh size, since the original large aggregate is broken down into smaller clusters or aggregates. This demonstrates that the size of the temporary small aggregate or cluster created immediately after filtering influences the final remade aggregate size.

The 11 μm pore size case is of particular interest because it is less than the average diameter of a B cell. Clusters in the filtrate are very small; primarily, cells are associated with only one backpack. This result suggests that even though a cell was forced to deform as it passed through the pore, the backpack remained on the surface. While this does not directly correlate to the active, receptor-mediated process of extravasation,[24] it does suggest that the cell−backpack association is sufficient to resist moderately strong mechanical challenges.

Conclusions

Cellular backpacks may be used to create aggregates of a model B-lymphocyte cell line. Two variables were examined to affect the size of the aggregates: the ratio of cells to backpacks, and the backpack diameter. By decreasing the ratio R of cells to backpacks, we increase the size of the aggregate. As the diameter of the backpack increases (for the same R), so does the aggregate size. Flow cytometry results indicate that for $R = 0.1$ and $d = 7$ μm, greater than 65% of cells will be associated with a backpack. When d increases to 15 μm at $R = 0.1$, greater than 45% of cells will remain attached to a backpack. When aggregates formed with $d = 7$ μm backpacks are forced through a mesh filter for varying pore sizes, aggregates will dissociate and reassociate. As the pore size decreases, the final aggregate size decreases as well. For the smallest pore size, 11 μm, backpacks remain associated with cells even though this is less than the diameter of the cell, suggesting a strong interaction between the cell and backpack.

Supporting Information Available. Details on photolithographic fabrication, flow cytometry, and confocal microscopy for $R = 10-3$ for $d = 7$ μm backpacks and laser diffraction data showing the agitation-dependent dissociation of aggregates. This material is available free of charge via the Internet at http://pubs.acs.org.

References and Notes

(1) Yoshida, M.; Roh, K. H.; Mandal, S.; Bhaskar, S.; Lim, D. W.; Nandivada, H.; Deng, X. P.; Lahann, J. *Adv. Mater.* **2009**, *21*, 4920–4925.

(2) Feinberg, A. W.; Feigel, A.; Shevkoplyas, S. S.; Sheehy, S.; Whitesides, G. M.; Parker, K. K. *Science* **2007**, *317*, 1366–1370.

(3) Ebara, M.; Yamato, M.; Aoyagi, T.; Kikuchi, A.; Sakai, K.; Okano, T. *Biomacromolecules* **2004**, *5*, 505–510.

(4) Okajima, S.; Sakai, Y.; Yamaguchi, T. *Langmuir* **2005**, *21*, 4043–4049.

(5) Kriha, O.; Becker, M.; Lehmann, M.; Kriha, D.; Krieglstein, J.; Yosef, M.; Schlecht, S.; Wehrspohn, R. B.; Wendorff, J. H.; Greiner, A. *Adv. Mater.* **2007**, *19*, 2483–2485.

(6) Cheng, H.; Kastrup, C. J.; Ramanathan, R.; Siegwart, D. J.; Ma, M.; Bogatyrev, S. R.; Xu, Q.; Whitehead, K. A.; Langer, R.; Anderson, D. G. *ACS Nano* **2010**, *4*, 625–631.

(7) Swiston, A. J.; Cheng, C.; Um, S. H.; Irvine, D. J.; Cohen, R. E.; Rubner, M. F. *Nano Lett.* **2008**, *8*, 4446–4453.

(8) Suematsu, S.; Watanabe, T. *Nat. Biotechnol.* **2004**, *22*, 1539–1545.

(9) Mendichi, R.; Soltes, L.; Schieroni, A. G. *Biomacromolecules* **2003**, *4*, 1805–1810.

(10) Kasaai, M. R.; Charlet, J. A. G. *J. Polym. Sci., Polym. Phys.* **2000**, *38*, 2591–2598.

(11) Tompkins, H. G.; Irene, E. A. *Handbook of Ellipsometry*; William Andrew Publishing and Springer-Verlag GmbH & Co.: Norwich, NY and Heidelberg, Germany, 2005.

(12) Agrawal, Y. C.; McCave, I. N.; Riley, J. B. *Principles, Methods, and Applications of Particle Size Analysis.*; Cambridge University Press: Cambridge, 1991.

(13) ShaikhMohammed, J.; DeCoster, M. A.; McShane, M. J. *Biomacromolecules* **2004**, *5*, 1745–1755.

(14) ShaikhMohammed, J.; DeCoster, M. A.; McShane, M. J. *Langmuir* **2006**, *22*, 2738–2746.

(15) Cho, J.; Char, K.; Hong, J. D.; Lee, K. B. *Adv. Mater.* **2001**, *13*, 1076–1078.

(16) Izquierdo, A.; Ono, S. S.; Voegel, J. C.; Schaaf, P.; Decher, G. *Langmuir* **2005**, *21*, 7558–7567.

(17) Krogman, K. C.; Lowery, J. L.; Zacharia, N. S.; Rutledge, G. C.; Hammond, P. T. *Nat. Mater.* **2009**, *8*, 512–518.

(18) Schlenoff, J. B.; Dubas, S. T.; Farhat, T. *Langmuir* **2000**, *16*, 9968–9969.

(19) Dubas, S. T.; Schlenoff, J. B. *Macromolecules* **1999**, *32*, 8153–8160.

(20) Kharlampieva, E.; Sukhishvili, S. A. *Polym. Rev.* **2006**, *46*, 377–395.

(21) Shiratori, S. S.; Rubner, M. F. *Macromolecules* **2000**, *33*, 4213–4219.

(22) Anderson, J. M.; Shive, M. S. *Adv. Drug Delivery Rev.* **1997**, *28*, 5–24.

(23) Schild, H. G.; Tirrell, D. A. *J. Phys. Chem.* **1990**, *94*, 4352–4356.

(24) Schenkel, A. R.; Mamdouh, Z.; Chen, X.; Liebman, R. M.; Muller, W. A. *Nat. Immunol.* **2002**, *3*, 143–150.